3

An Anisotropic Behaviour Analysis of AA2024 Aluminium Alloy Undergoing Large Plastic Deformations

Adinel Gavrus and Henri Francillette
European University of Brittany, National Institute of Applied Sciences, Rennes France

1. Introduction

The mechanical behaviour of metals during real forming processes must be related to their anisotropic properties. Concerning the analysis of the anisotropic behaviour of aluminium alloys this one has been the subject of various studies, generally in the field of sheet forming processes ((Malo *et al.,* 1998), (Lademo *et al.,* 1999)). In the last decades the majority of the fundamentals works search to define the mathematical description of the anisotropy starting from modified quadratic Hill criteria, non-quadratic ones such as Cazacu-Barlat (Cazacu & Barlat, 2001), Banabic (Banabic, 2002) or other sophisticated models synthesized in (Khalfallah, 2004). On the experimental point of view the many researches describe the rolled sheet properties of aluminium alloys (Choi & Barlat, 1999), (Li *et al.,* 2004), (Park, 1999)) and report the anisotropic response during the mechanical deformation from uniaxial tensile tests, wire drawing or simple shear ones ((Fjeldl & Roven , 1996), (Hu *et al.,* 1998), (Lloyd & Kenny, 1980), (Yonn, 2005)). Until now relatively few studies concerns the use of the channel die compression test, where deformation history is close of the principal sheet forming process such as the cold rolling one (Francillette *et al.,* 1998).

In this study an aluminium alloy (AA2024) is analyzed in order to characterize its anisotropy and its mechanical behaviour with this latter mechanical test. In a first part, the microstructure of the material is defined through optical and SEM microscopy, EBSD and X ray measurements. Micro-macro approaches will be used to valid the experimental measurements. Next, mechanical tests mainly the channel die compression one (see Francillette *et al,* 2003) and the tensile one are used in order to determine the macroscopic anisotropic behaviour of the material. A rigorous analytical model, able to describe the large plastic deformation of the material specimen which occurs during these experimental tests, will be developed. The main idea consist to define analytical equations which permits to compute the stress, the plastic strain rate and the cumulated plastic strain corresponding to a parallelepiped material undergoing a channel die upsetting loading. Final formula will be established to compute all the coefficients corresponding to a quadratic Hill criterion. A comparison with the well known computation model corresponding to the tensile test will be made. Next, a more general Hill criterion, taking into account variation of its coefficients with the plastic strain, will be analyzed. Starting from the previous mathematical description, a general methodology, able to identify rigorously all the parameters defining

the laws of variation of the computed quantities with the plastic strain, will be presented. Finally an application for a plan and normal anisotropic formulation, corresponding to AA2024 aluminium alloy rolled plate, will be detailed. A new approach will be then proposed in order to predict the Lankford coefficient values and a validation will be made by a comparison of these ones with those obtained from classical tensile tests.

2. Experimental analysis

Aluminium alloys present specific microstructures according to their chemical composition. These alloys are classified in several series as indicated in Table 1, according to the main elements of their chemical composition.

Series	1000	2000	3000	4000	5000	6000	7000
Composition	Al	Al-Cu	Al-Mn	Al-Si	Al-Mg	Al-Mg-Si	Al-Zn-Mg

Table 1. Chemical composition of aluminium alloys: xxxx series.

They can be shared out in two categories: those which do not present structural hardening (Al, Al-Mn, Al-Mg) and those which present structural hardening (Al-Cu, Al-Mg-Si, Al-Zn-Mg). The different phases which may be present in each series have been reported in (Barralis & Maeder, 2005). The chemical composition strongly favors the presence or not of precipitates during the elaboration process. In this paper anisotropic behaviour of an AA2024 aluminium alloy of 2000 series will be analyzed. Parallelepiped samples were cut out from a starting sheet with a thickness equal to 8.4 mm using the following dimensions: l_0 = 11 mm, w_0 = 10 mm and h_0 = 8.4 mm, where l_0, w_0 and h_0 are the initial length, width and respectively the high of the specimen. The initial rolling, transverse and normal directions of the sheet are defined by RD_0, TD_0 and ND_0. We will call LD, TD and ND the longitudinal, transverse and respectively normal directions corresponding to a channel die device (Fig. 1).

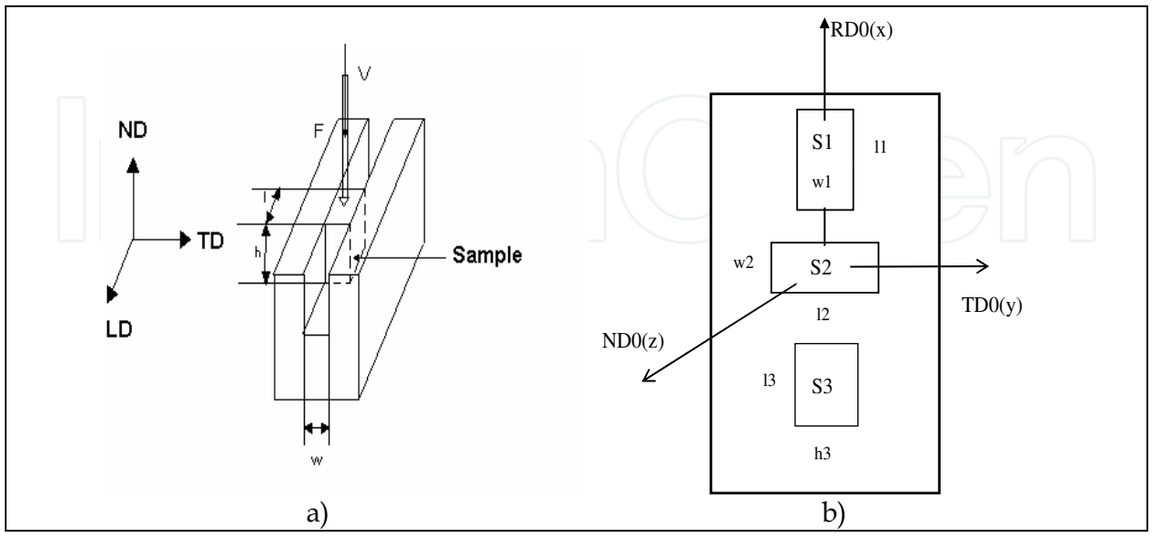

Fig. 1. The channel die compression test: a) device scheme, b) the initial sheet and the cut of the samples (S1, S2 and S3).

For the analysis of the mechanical behaviour of the material, channel die compression tests have been carried for three different specimens. The samples were positioned in the device and cut out from the initial sheet so that:

- LD // RD_0 ; TD // TD_0 ; ND // ND_0 (specimen S_1 and position 1)
- LD // TD_0 ; TD // RD_0 ; ND // ND_0 (specimen S_2 and position 2)
- LD // RD_0 ; TD // ND_0 ; ND // TD_0 (specimen S_3 and position 3)

For the specimen S_3 the following dimensions are chosen: l_0 = 11 mm, w_0 = 8 mm and h_0 = 10 mm. During the mechanical tests the strength is applied along the ND direction with a constant speed V closed to 2.10^{-2} mm/s and the sample is extended along the LD direction without displacement along the TD one. On the other hand, the coefficient of plan anisotropy r(θ) during plastic deformation is also determined starting from the ratio between the measured width reduction and the thickness one and using different orientations of specific tensile specimens cut out from the initial sheet (Banabic, 2000). The angle θ permits to describe the orientation of the specimen with respect to the initial rolling direction and its values chosen in this study are: θ = 0°, 30°, 45°, 60°, 90°. All the specimens were mechanically polished with abrasive paper and a solution with a chemical composition of 64% H_3PO_4, 27% H_2SO_4 and 9% NH_3 was systematically used for surfaces preparation. Different experimental techniques were used for the characterization of the material: optical microscopy, SEM, EBSD and X ray diffraction. The crystallographic textures have been characterized by the measurement of the {111}, {200} and {220} pole figures using the $K\alpha_1$ copper radiation (λ =1.54056). In a next part, the stress-strain curves are determined to highlighting the difference between the mechanical responses of the deformed samples.

3. Preliminary results and comments

In Figure 2, an illustration of the initial microstructure of the AA2024 of this study is presented using optical microscopy (Fig. 2a) and the Scanning Electron Microscope (Fig. 2b).

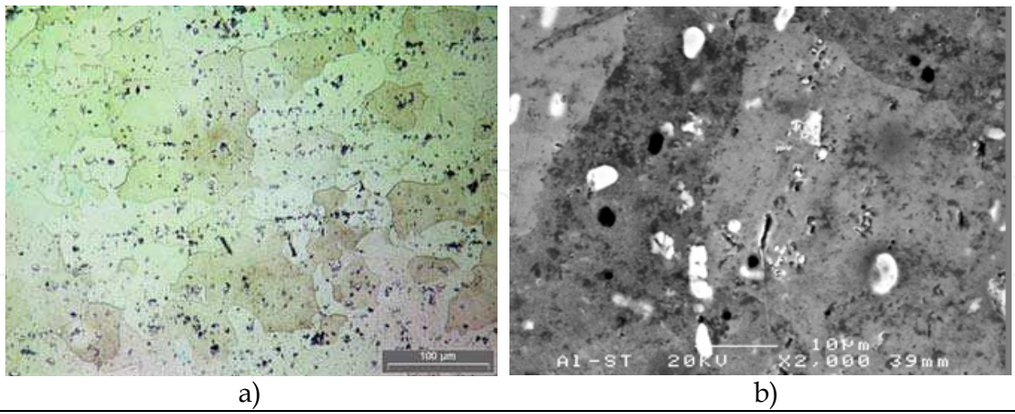

a) b)

Fig. 2. Initial microstructure of the material: a) Optical micrograph, b) SEM characterization - (Al, Cu) precipitates.

It is then possible to see that the size of the grains is not homogeneous: some grains have a size larger than 100 µm and other grains lower than 80 µm. At a finer scale, the observation with the SEM indicates the presence of precipitates (bright points) which are (Al, Cu) precipitates according to EDS analysis. The metallurgical quantities which define the

microstructure of aluminium alloys (gain size, precipitates, dislocations …) are important elements for interpreting the mechanical behaviour. During the elaboration of the material, thermo-mechanical treatments are generally chosen in order to optimize the mechanical properties and the microstructure. Other quantity necessary to understand the mechanical characterization is the crystallographic texture. Deformation, recrystallisation, solidification during thermomechanical processes contribute to the development of this type of texture ((Lücke & Engler, 1990), (Browen, 1990), (Zeng *et al.*, 1994), (Engler, 1994), (Engler, 1995)). To define it for a polycrystalline material, it is necessary to describe the orientation of a particular grain through the Miller indices. For example, in rolling, the (*hkl*)[*uvw*] component corresponds to the (*hkl*) plane parallel to the rolling plane and to the [*uvw*] direction parallel with the rolling direction. The correspondences between the Euler angles and the Miller indices can be found in the literature (Hansen, 1978). For the description of the crystallographic orientation of a particular grain of a textured material, it is necessary to consider a reference system (C_1, C_2, C_3) placed on three characteristic directions of the crystal lattice that are normal to each other, for example <100> directions in cubic metals. Let also consider a sample reference system defined by three directions (X, Y, Z), usually the rolling direction (RD), the transverse direction (TD) and the normal direction to the rolling plane (ND). The description of the crystallite orientation with respect to X, Y, Z is often done by the three Euler angles ϕ_1, ϕ and ϕ_2. At the initial stage, the two coordinate systems are coincidental (X along C_1, Y along C_2 and Z along C_3). The sample system is firstly rotated by a ϕ_1 angle around Z, next, a rotation of ϕ angle is applied around C_1 and, a thirdly, a successive rotation of ϕ_2 around C_3 bring the crystal orientation in its final position, as indicated Figure 3 (Bunge, 1996). Theoretically, ϕ_1 and ϕ_2 may vary from 0° to 360° and ϕ from 0° to 90°. By symmetry, the three angles may be considered between 0° and 90°.

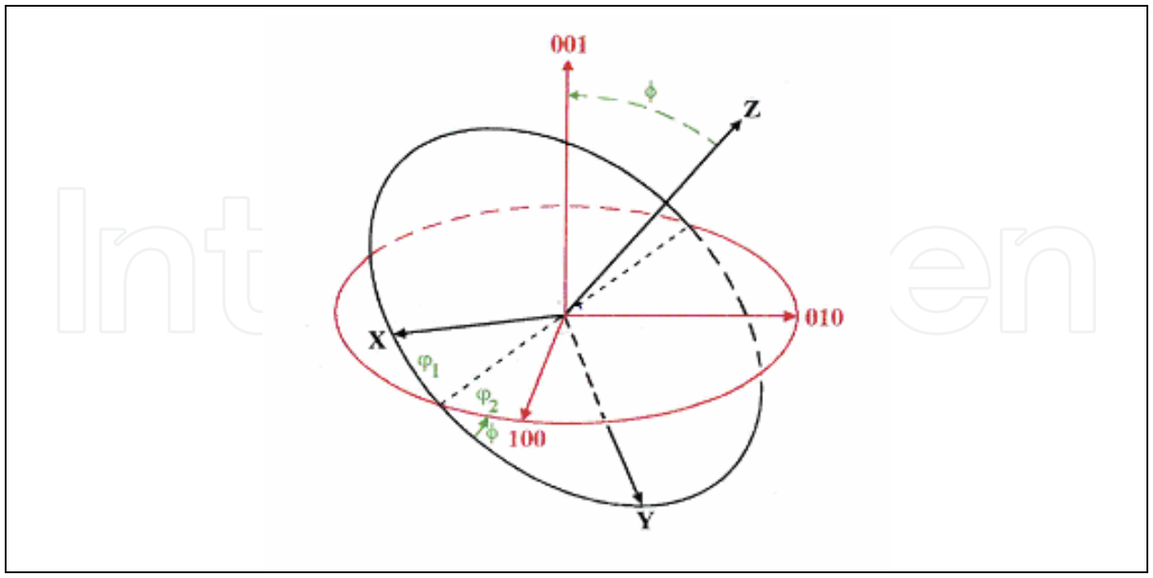

Fig. 3. Definition of the Euler angles.

The matrix transformation which relates the two coordinates systems (X, Y, Z) and (C_1, C_2, C_3) has an expression given by the composition of three elementary rotations:

$$\begin{pmatrix} \cos\phi_1\cos\phi_2 - \sin\phi_1\sin\phi_2\cos\phi & \sin\phi_1\cos\phi_2 + \cos\phi_1\sin\phi_2\cos\phi & \sin\phi_2\sin\phi \\ -\cos\varphi_1\sin\varphi_2 - \sin\phi_1\cos\phi_2\cos\phi & -\sin\phi_1\sin\phi_2 + \cos\phi_1\cos\phi_2\cos\phi & \cos\phi_2\sin\phi \\ \sin\phi_1\sin\phi & -\cos\phi_1\sin\phi & \cos\phi \end{pmatrix} \quad (1)$$

Different techniques may be used for the experimental determination of the crystallographic texture of the material. Among them, one local technique which can afford an orientation mapping of neighbouring grains is the Electron Back Scattering Diffraction (EBSD), in a SEM. Figure 4 presents an example of an experimental diffraction pattern with its indexation.

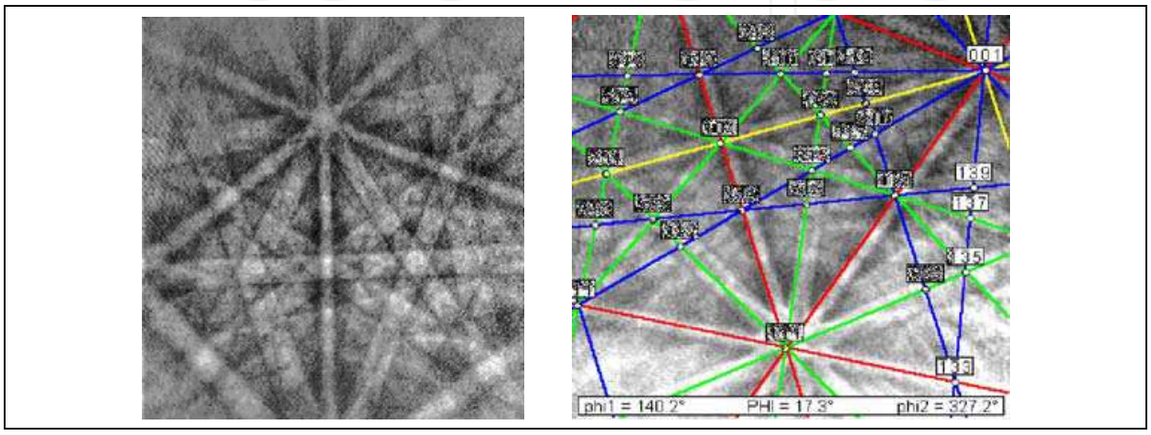

Fig. 4. Example of the diffraction pattern using EBSD technique.

With this technique the individual matrix g expressed by relation (2) are determined for the different particular points. Next, each grain can be compared with its neighbourhood. Figure 5 present then an illustration of a crystallographic experimental determination carried out on the AA2024 alloy using EBSD map determined to precise the neighbouring of the grains necessary for a local characterization of the crystallographic orientations of the starting material (Fig. 5b).

In Fig. 5b the map corresponds to a zone of approximately (200 μm x 570 μm) and the result is consistent with the optical characterization which shows grains greater than the others.

Other possible way to characterize the grain orientations of the material uses X-ray diffraction measurements for the texture determination. Let g be the crystal orientation noted $g = (\phi_1, \phi, \phi_2)$ and dg an infinitesimal range around it. The Orientation Distribution Function (ODF), F(g), is the continuous function which describes the crystallographic texture ((Bunge, 1996), (Bunge & Schwarzer, 1998)). By definition, F(g)dg is the volume fraction of all crystallites for which the g crystal orientation is in the dg range :

$$F(g)dg = dV(g)/V \; ; \; g = (\phi_1, \phi, \phi_2) \quad (2)$$

F(g) is determined from pole figure measurements and background and defocusing corrections.

From the knowledge of ODF complete recalculated poled figures can be determined. As an illustration the crystallographic texture of the aluminium alloy reported in this study have been characterized by the measurement of the {111}, {200}, and {220} pole figures using the

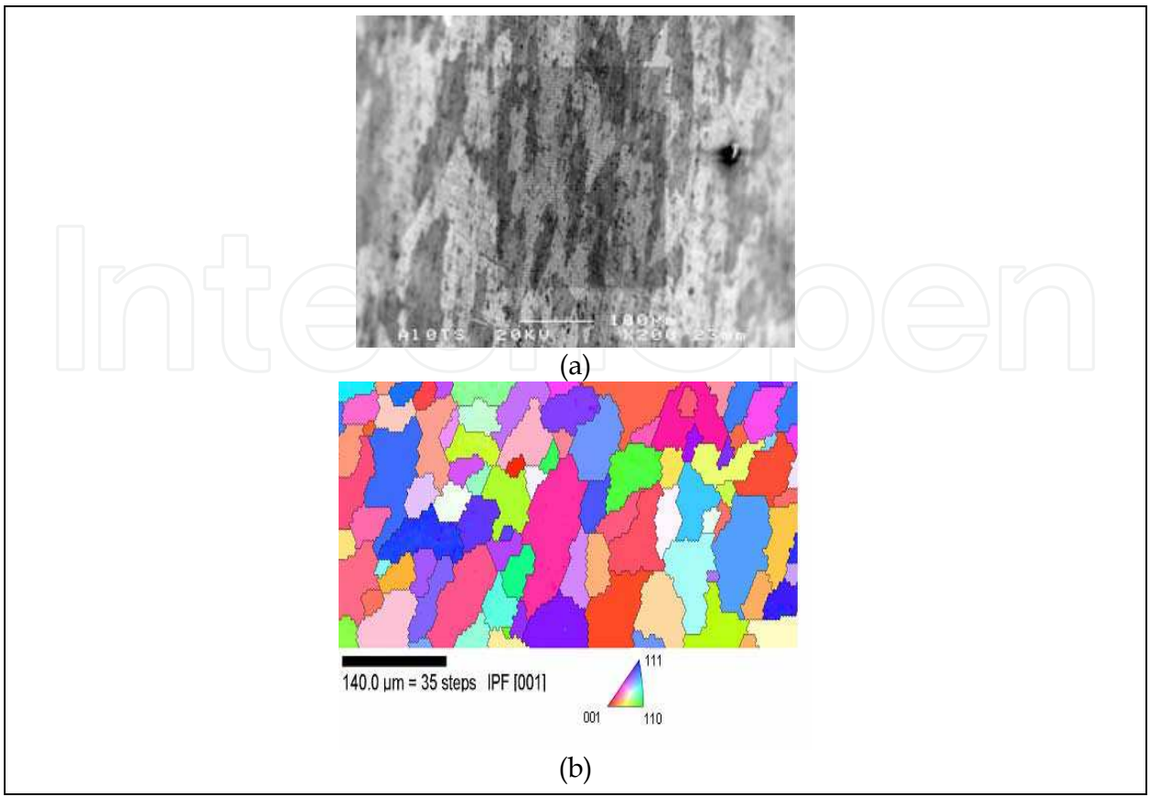

Fig. 5. Crystallographic characterization of the AA2024 alloy with the EBSD technique in the SEM: (a) the sample surface characterization, (b) crystallographic map of the material.

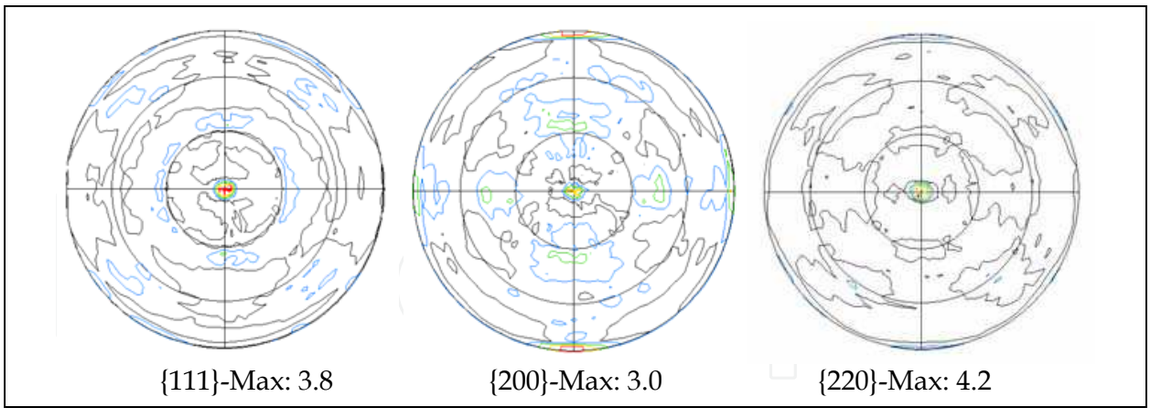

Fig. 6. Initial texture of an AA2024 aluminium alloy: {111}, {200} and {220} recalculated pole figures.

$K_{\alpha 1}$ copper radiation (λ =1.54056 Å). Concerning the initial texture (XR characterization), the {111}, {200} and {220} pole figures corresponding to the initial state of the material are presented in Fig. 6. The recalculated pole figures use the corrections mentioned above.
From these preliminary experimental results it is possible to conclude that the studied material has three principal initial textures and the choice of the three specimen positions is then valid. Moreover these figures are particularly important to determine the evolution of

the orientation of the grains with the plastic deformation. Then the microscopic phenomenon which accompanies the plastic deformation and the stress state in aluminium alloys is the accumulation of dislocations in the material. This contributes to the formation of three-dimensional arrays that depend on strain, strain rate, chemical composition, stacking fault energy, temperature and loading path. The chemical composition is particularly important since for pure aluminium, solute or dispersion strengthened aluminium alloys might exhibit different microstructural features. For instance, pure aluminium is a cell forming material ((Hansen, 1991), (Hansen, 1992), (Lopes *et al.*, 2003)). But Al-Mg is a non cell forming metal ((Hughes, 1992), (Hughes, 1993)). On the other hand, for alloys such as Al-Cu, Al-Mg-Si, Al-Cu-Mg, the description of the microstructure may be more complex because of the presence of alloying elements in solid solution, the precipitates and their interactions with the dislocations (Baudelet *et al.*, 1978). In the mechanical behaviour of these materials, strain hardening is the consequence of the increase of dislocation density which interacts with geometric hardening due to texture change. Generally the grains tend to rotate towards more stable orientations. For aluminium alloys, after hot or cold rolling conditions, the {112}<111> (Copper), {110}<112> (Brass) and {123}<634> (S) orientations are dominant components. The proportions between these different components depend on the rolling conditions and material composition. However, after an annealing treatment, depending on the process conditions, the texture can be nearly isotropic or composed of the following components: {100}<001> (Cube) and {110}<001> (Goss). The positions of important orientations in Euler angle space are listed in the Table 2.

Name	{hkl}	<uvw>	ϕ_1	ϕ	ϕ_2
C	112	111	90	35	45
D	4 4 11	11 11 8	90	27	45
S	123	523	55	37	63
G	011	100	0	45	90
B	011	211	35	45	90
B/G	~011	411	20	45	90

Table 2. The important orientations defined in the Euler angle space (first subspace).

At ambient temperature, the copper type is characteristic for materials with high or intermediate stacking fault energy. On the other hand, the brass type behaviour is characteristic for materials with low stacking fault energy. Important parameters which introduce modifications from one type to texture to and other type are the temperature (particularly for rolling) and the strain rate ((Hu & Cline, 1961), (Hu & Goodman, 1963)). Slip on {111}<110> systems is significant in these alloys and explain the formation of texture. However in the literature there are indications that other slip planes than {111} may be active in fcc alloys. Consequently some authors suggest that non octahedral slip may explain texture formation (Bacroix & Jonas, 1998).

The crystallographic textures of the samples after the plastic deformation are characterized in Fig. 7. This figure pictures the {111}, {200} and {220} pole figures of the AA2024 aluminium alloy after deformation by channel die compression test (specimens S1, S2 and S3). The comparison of the different pole figures indicates that the average orientation of the grains of S_1 and S_2 are similar. This result is consistent with the stress levels measured in the ND direction for these two specimens (614.37 MPa for S1 and 614.05 MPa for S2). Moreover

the measured pole figures seem to be consistent with those determined in aluminium alloys during a cold rolling ((Leacock, 2006), (Huh *et al.,* 2001), (Jin & Lloyd, 2005)).

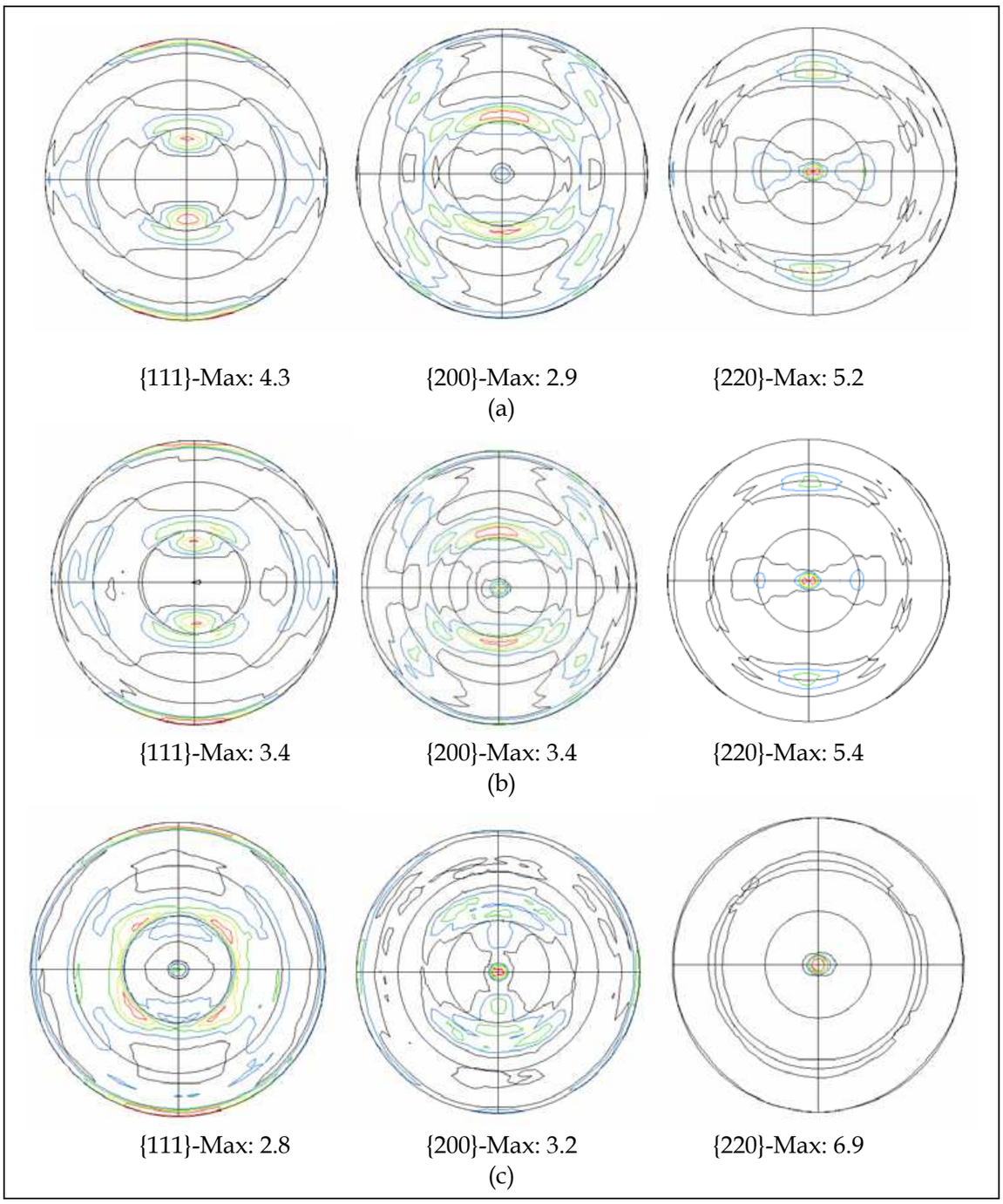

Fig. 7. Experimental textures of the AA2024 alloy after channel die compression tests: {111}, {200} and {220} recalculated pole figures for: (a) LD // RD_0, TD // TD_0, ND // ND_0 (deformed specimen S1), (b) LD // TD_0, TD // RD_0, ND // ND_0 (deformed specimen S2), (c) LD // RD_0, TD // ND_0, ND // TD_0 (deformed specimen S3).

This figure pictures the {111}, {200} and {220} pole figures of the AA2024 aluminium alloy after deformation by channel die compression test (specimens S1, S2 and S3). The comparison of the different pole figures indicates that the average orientation of the grains of S_1 and S_2 are similar. This result is consistent with the stress levels measured in the ND direction for these two specimens (614.37 MPa for S1 and 614.05 MPa for S2). Moreover the measured pole figures seem to be consistent with those determined in aluminium alloys during a cold rolling ((Leacock, 2006), (Huh *et al.,* 2001), (Jin & Lloyd, 2005)).

4. Micro-Macro approach

The mechanical behaviour of aluminium alloys are related to their texture evolutions. Several polycrystalline models have been developed to interpret the experimental observations from the active deformation slip systems. The first one is the Sachs model which assumes the same form for the stress state in each grain (Sachs, 1928). The slip systems are activated when the maximum shear stresses are reached according to the Schmid's law:

$$\sigma_{ij}.m_{ij}^{s} = \tau_c^s \tag{3}$$

where m_{ij}^{s} is the generalized Schmid factor defined by :

$$m_{ij}^{s} = \frac{1}{2}(n_i^s b_j^s + b_i^s n_j^s) \tag{4}$$

Here $\vec{n}^s$ is the unitary slip plane normal of the *s* systems and $\vec{b}^s$ is the unitary slip direction of the system: *s* varies from 1 to 12 for aluminium alloys. With this model, the deformation is different from grain to grain in the polycrystalline material.
On the other hand, the Taylor model considers that the strain tensor is the same in all the grains of the polycrystalline material (Taylor, 1938). Five slip systems are necessary for a prescribed strain increment. The selection of these systems among several possibilities is achieved with the application of the criterion of minimum internal work:

$$\text{Min of } \sum_s \tau_c^s.\dot{\gamma}^s \tag{5}$$

where $\dot{\gamma}^s$ is the shear rate on the active *s* system.
Bishop and Hill (Bishop et al., 1951), (Bishop, 1953)) determined all the possible stress states for five independent slip systems in the five dimensional space of the components of the stress tensor. They used the criterion of the maximum external work to select the appropriated stress state:

$$\text{Max of } \sum \sigma_{ij}\dot{\varepsilon}_{ij} \tag{6}$$

with $\dot{\varepsilon}_{ij}$ given by:

$$\dot{\varepsilon}_{ij} = \sum_s m_{ij}^{s}\dot{\gamma}^s \tag{7}$$

It can be shown that the Taylor theory and the Bishop-Hill theory are mathematically equivalent. Both criteria (5) and (6) have been shown to lead to the same results. From the

Taylor model, relaxed constraints models have also been developed for more accurate predictions of texture evolutions ((Hirsch & Lücke, 1988)), (Engler *et al.*, 2005), (Molinari *et al.*, 1994)).
More complex models which take into account the active slip systems of the material and the interaction between the grains have been applied to the characterization of anisotropy, notably the viscoplastic self consistent models (VPSC). In their approach, Molinari *et al.* (1994) derived the following interaction law by considering the concept of Homogeneous Equivalent Matrix (HEM) and 1-site approximation:

$$s^g - \mathrm{S} = \left(\Gamma^{gg'-1} + \mathrm{A}\right) : (\dot{\varepsilon}^g - \dot{\mathrm{E}}) \tag{8}$$

where S and $\dot{\mathrm{E}}$ are respectively the deviator stress tensor and the strain rate tensor at the macroscopic level. S^g and $\dot{\varepsilon}^g$ represent the same quantities at the grain scale. The interaction tensor Γ between a grain g and its neighbourhood described by g' can be obtained by integration of the symmetric part of the second derive of the Green function. It can take into account the effect of grain shape (spherical or ellipsoidal).
In the model, the microscopic strain rate is calculated using a viscoplastic power law relation:

$$\tau^s = \tau_0^s \left(\frac{\dot{\gamma}^s}{\dot{\gamma}_0^s} \right)^n \tag{9}$$

Then, using (7) it can be written:

$$\dot{\varepsilon}_{ij} = \dot{\gamma}_0 \sum_s m_{ij}^s \left(\frac{s_{kl} m_{kl}}{\tau_0^s} \right)^{\frac{1}{n}} \tag{10}$$

Lebensohn & Tomé (1993) have also developed a VPSC approach to predict the mechanical behaviour of polycrystalline materials. They derived the following interaction relation:

$$\dot{\varepsilon} - \dot{\mathrm{E}} = -\tilde{\mathrm{M}}(s - S) \tag{11}$$

The tensor $\tilde{\mathrm{M}}$ characterizes the interaction between a grain and its neighbourhood.
These micro-macro models have also been used for the determination of the anisotropy of aluminium alloys. They present the advantage to relate the mechanical behaviour of the material to the physical mechanisms of deformation. Some authors have compared experimental measurements of the flow stress and the Lankford coefficient (r-value) with the predictions of the full constraints and relaxed constraints Taylor-Bishop-Hill models ((Kuwabara *et al.*, 2002), (Fjeldly & Roven, 1996)). These comparisons are often carried out for different angles between the tensile axe and the initial rolling direction of the material. Other important application of these models in the characterization of the anisotropy of aluminium alloys is the prediction of the yield loci for different texture components ((Lequeu *et al.*, 1987), (Hu *et al.*, 1998)). In a comparative study Choi and Barlat ((Choi & Barlat, 1999), (Choi *et al.*, 2000)) showed that their experimental results are in better agreement with the VPSC approach than the Taylor one. A complementary analysis of the anisotropy of an AA1050 aluminium sheet has been carried out also by Lopes *et al.* (2003) for

the description of tensile and simple shear stress strain curves with the VPSC model developed by Lebensohn & Tomé (1993). The authors modeled the macroscopic curves by indentifying the parameters describing strain hardening on the slip systems.
From the measurement of the pole figures of the material of this study and the determination of the ODF at the initial stage, the coefficient of anisotropy, obtained from the ratio between the measured width reductions and the high ones, has been calculated with the Taylor FC model and the VPSC developed by Lebensohn and Tomé for different angles between the tensile axis and the specimen. The results are presented in Figure 8.

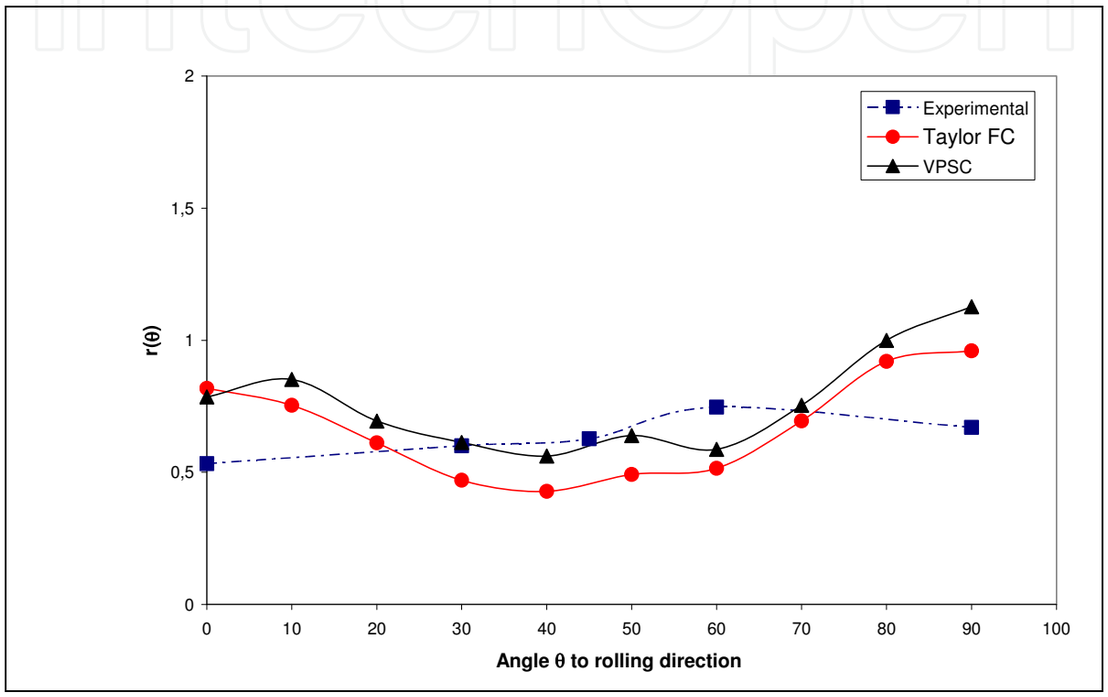

Fig. 8. The coefficient of the anisotropy r(θ) value versus angle θ defining orientation to the initial rolling direction of the starting sheet: experimental and computed values determined with the Taylor FC and the VPSC models.

The two models predict values close to the experimental ones and the differences are relatively low between 20°-70°.

5. Classical analysis of anisotropic behaviour

This paper proposes to analysis the anisotropic behaviour assuming the orthotropic symmetry hypothesis and using the most known quadratic criterion such as the classical Hill one (Hill, 1948) defined by:

$$f([\sigma]) = F(\sigma_{yy} - \sigma_{zz})^2 + G(\sigma_{zz} - \sigma_{xx})^2 + H(\sigma_{xx} - \sigma_{yy})^2 + 2L\sigma_{yz}^2 + 2M\sigma_{zx}^2 + 2N\sigma_{xy}^2 - 1 = 0 \quad (12)$$

According to the basic scientific literature, the Hill coefficients can be defined from simple tensile tests and simple shear ones using the following relationships:

$$F = \frac{1}{2}\left[\frac{1}{\sigma_{0yy}^2}+\frac{1}{\sigma_{0zz}^2}-\frac{1}{\sigma_{0xx}^2}\right], G = \frac{1}{2}\left[\frac{1}{\sigma_{0xx}^2}+\frac{1}{\sigma_{0zz}^2}-\frac{1}{\sigma_{0yy}^2}\right], H = \frac{1}{2}\left[\frac{1}{\sigma_{0yy}^2}+\frac{1}{\sigma_{0xx}^2}-\frac{1}{\sigma_{0zz}^2}\right] \quad (13)$$
$$L = \frac{1}{2\sigma_{0yz}^2}, M = \frac{1}{2\sigma_{0zx}^2}, N = \frac{1}{2\sigma_{0xy}^2}$$

where σ_{0xx} , σ_{0yy} , σ_{0zz} represent the yield stress corresponding to each tensile direction and σ_{0xy} , σ_{0yz} , σ_{0zx} are the critic shear stress.

If a plan anisotropy of the material sheet is assumed, the expression of the coefficient of anisotropy r(θ), expressing the ratio between the width reduction and the thickness one, can be defined analytically by:

$$r(\theta) = \frac{\dot{\varepsilon}_{yy}}{\dot{\varepsilon}_{zz}} = \frac{H + (2N - F - G - 4H)\sin^2(\theta)\cos^2(\theta)}{F\sin^2(\theta) + G\cos^2(\theta)} \quad (14)$$

In this case is possible to estimate the Hill coefficients directly from the measured anisotropic coefficient r(θ) i.e.:

$$r(0) = R = \frac{H}{G}, r(45) = \frac{1}{2}\left(\frac{2N - F - G}{F + G}\right), r(90) = \frac{H}{F}, H = \frac{R}{R+1}\frac{1}{\sigma_{0xx}} \quad (15)$$

Regarding the Fig. 8, the measured values of the plastic strain ratio defined by (14) shows that *r(θ)* increase with the rolling direction θ for most of the experimental points. The greatest measured value is determined for θ = 60°. Values of the coefficient of anisotropy lower than 1 are reported in literature for aluminium alloys ((Leacock, 2006), (Choi *et al.*, 2000), (Choi *et al.*, 2001), (Tong, 2006)). Moreover the variation measured in the study is consistent with the experimental data of Leacock (Leacock, 2006) for an AA2024 alloy. Despite the particular value for the 60°, all the other values are between 0.540 and 0.654. Moreover $\bar{r} = 0.62$, $\Delta r = -0.04$ and it can be concluded that these quantities permits to consider that the plate have a normal anisotropy described by:

$$\sigma_{xx}^2 + \sigma_{yy}^2 - \frac{2R}{R+1}\sigma_{xx}\sigma_{yy} + \frac{2(2R+1)}{R+1}\sigma_{xy}^2 = \frac{R}{H(R+1)} = \sigma_0^2 \quad (16)$$

It is important to note that in all the literature the use of the tensile test and the computation of the anisotropic coefficients are used without the take into account the variation of the yield stress with the plastic deformation. Moreover, because of the striction phenomenon, the tensile test is limited to small plastic deformation (around of 15% for aluminium alloy).

For an anisotropic behaviour analysis corresponding to large plastic deformation conditions, this paper proposes the use the channel die compression experiments. The corresponding stress-strain curves determined from the three different sample positions defined in §2 (according to the three types of observed textures), are presented in Fig. 9.

Using the general law proposed by Gavrus (Gavrus, 1996) and using only influence of the cumulated plastic strain the following expression can be used to fit the above experimental curves:

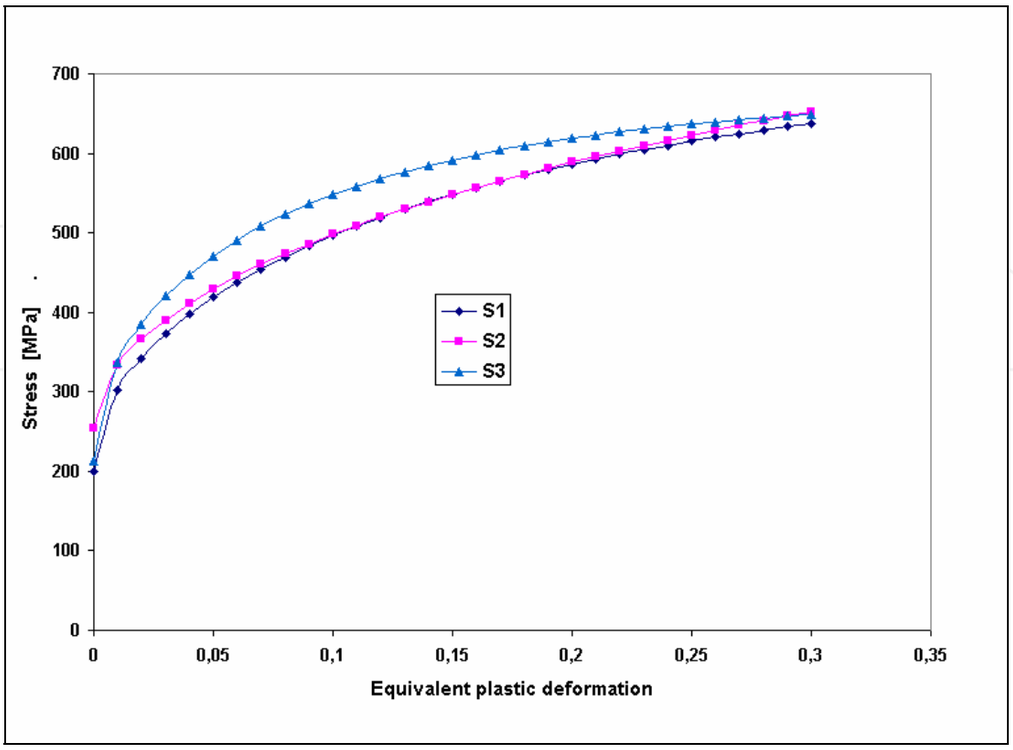

Fig. 9. Experimental stress strain curves of the specimens (S_1, S_2, S_3) deformed by channel die compression.

$$\sigma = \sigma_{00} + \sigma_{pl}\left[1 - \exp(-n\bar{\varepsilon})\right]^{n_a} W + \sigma_{sat}\left[1 - W\right] \quad \text{with} \quad W = \exp\left(-r\bar{\varepsilon}^{s}\right) \tag{17}$$

It have been shown that this formulation is able to describe different shapes of the stress-strain curves and can explain observed physical phenomena such as the hardening, the dynamic recovery, the dynamic softening or the break slope one. It is worth noting that the curves are similar for S_1 and S_2: the stress levels are close to each other in the main part of the plastic deformation. Concerning S_3, the stress levels are more important. For instance, at 15% of the plastic deformation, the normal stress is 548 MPa for S_1, S_2 and 591 MPa for S_3.

6. The analytical model describing the channel die compression test

The main advantage of the channel die compression test is the homogeneity of the plastic deformation caused by the small effect of the friction (if a teflon material is used on the tool-specimen interfaces) and the absence of the shape instability caused by the striction phenomenon (important for the classical tensile test). Consequently an analytical model can be used to compute stress, strain and strain rate tensors. From our knowledge a similar approach has already been mentioned only for tensile tests (Liu *et al.*, 1997) using a phenomenological study of the anisotropic criterion. The present research work proposes a model based on the expression of the classical Hill criterion ((Hill, 1948), (Hill, 1979)) but introducing a variation of the Hill coefficients with a defined cumulated plastic strain. A parameter identification method based on an inverse analysis technique will be used to describe quantitatively the anisotropic model. We note *l*, *w*, *h* the length, width and

respectively the high of the samples during the mechanical test and *V* the punch compression speed. According to the channel die device axes: X(LD), Y(TD), Z(ND) defined in Fig.1, the kinematics conditions and the incompressibility equation ($\mathrm{div}(\vec{v})=0$) lead to the following form of the velocity vector:

$$\vec{v} = \begin{bmatrix} u(X) \\ 0 \\ w(Z) \end{bmatrix} = \begin{bmatrix} XV/h \\ 0 \\ -ZV/h \end{bmatrix} \tag{18}$$

Consequently we have a diagonal strain rate tensor $\dot{\varepsilon}$ for which the component in the Z direction is equal to -V/h, in the Y direction is equal to 0 and in the X direction is equal to V/h. To take into account the plastic strain history, a deformation tensor can be defined by:

$$\varepsilon = \int_0^t \dot{\varepsilon} dt = \begin{bmatrix} \int_0^t (V/h) d\tau & 0 & 0 \\ 0 & 0 & 0 \\ 0 & 0 & -\int_0^t (V/h) d\tau \end{bmatrix} \tag{19}$$

In a first approximation, an equivalent plastic strain value can be expressed in term of the second invariant of the deformation tensor i.e.:

$$\bar{\varepsilon} = \sqrt{\frac{2}{3}\mathrm{tr}\left(\varepsilon^2\right)} = \sqrt{\frac{2}{3}\left(\varepsilon_{xx}^2 + \varepsilon_{yy}^2 + \varepsilon_{zz}^2\right)} = \frac{2}{\sqrt{3}}\ln\left(\frac{h_0}{h}\right) \tag{20}$$

where h_0 is the initial height of the samples.

Because the deformation along the Y direction is rigorously equal to 0 ($\varepsilon_{yy} = \int_0^t \dot{\varepsilon}_{yy} dt = 0$) we obtain a plane strain deformation. The corresponding stress tensor is also diagonal and has a null component in the X direction (free plastic flow i.e. plan stress conditions):

$$\sigma = \begin{bmatrix} 0 & 0 & 0 \\ 0 & \sigma_{yy} & 0 \\ 0 & 0 & \sigma_{zz} \end{bmatrix} \text{ with } \sigma_{zz} = F/S \tag{21}$$

where $S = lw = (l_0 w_0) h_0/h$ is the area of the real sample surface in contact with the punch and *F* is the forging load measured in the Z direction.

Starting from this mathematical model of the plan compression experiment, the following expressions of the strain rate tensor and of the stress tensor are obtained for the three sample positions:

a. Position P1 (specimen S1)

$$[\dot{\varepsilon}] = \begin{bmatrix} V/h & 0 & 0 \\ 0 & 0 & 0 \\ 0 & 0 & -V/h \end{bmatrix}; [\sigma] = \begin{bmatrix} \sigma_{LD//RD_0}^{(1)} = 0 & 0 & 0 \\ 0 & \sigma_{TD//TD_0}^{(1)} & 0 \\ 0 & 0 & \sigma_{ND//ND_0}^{(1)} \end{bmatrix}$$

b. Position P2 (specimen S2)

$$[\dot{\varepsilon}]=\begin{bmatrix}0 & 0 & 0\\ 0 & V/h & 0\\ 0 & 0 & -V/h\end{bmatrix};\quad [\sigma]=\begin{bmatrix}\sigma^{(2)}_{TD//RD_0} & 0 & 0\\ 0 & \sigma^{(2)}_{LD//TD_0}=0 & 0\\ 0 & 0 & \sigma^{(2)}_{ND//ND_0}\end{bmatrix} \tag{22}$$

c. Position P3 (specimen S3)

$$[\dot{\varepsilon}]=\begin{bmatrix}V/h & 0 & 0\\ 0 & -V/h & 0\\ 0 & 0 & 0\end{bmatrix};\quad [\sigma]=\begin{bmatrix}\sigma^{(3)}_{LD//RD_0}=0 & 0 & 0\\ 0 & \sigma^{(3)}_{ND//TD_0} & 0\\ 0 & 0 & \sigma^{(3)}_{TD//ND_0}\end{bmatrix}.$$

The index (i) refers to the sample position and all the matrixes are written in the coordinates system of the sheet.

7. The anisotropic behaviour model

For standard materials, using a convex anisotropic yield function *f* expressed in terms of the stress tensor components, the strain rate matrices can be determined from the stress gradient of the convex surface:

$$[\dot{\varepsilon}]=\lambda^{pl}\frac{\partial f}{\partial[\sigma]} \tag{23}$$

where λ^{pl} is the plastic multiplier.
According to the Hill criterion defined in (12), for each strain rate component the following expressions can be written:

$$\begin{aligned}&\dot{\varepsilon}_{xx}=2\lambda^{pl}\left[G(\sigma_{xx}-\sigma_{zz})+H(\sigma_{xx}-\sigma_{yy})\right],\quad \dot{\varepsilon}_{yy}=2\lambda^{pl}\left[F(\sigma_{yy}-\sigma_{zz})+H(\sigma_{yy}-\sigma_{xx})\right]\\ &\dot{\varepsilon}_{zz}=2\lambda^{pl}\left[F(\sigma_{zz}-\sigma_{yy})+G(\sigma_{zz}-\sigma_{xx})\right],\quad \dot{\varepsilon}_{xy}=4\lambda^{pl}N\sigma_{xy},\ \dot{\varepsilon}_{yz}=4\lambda^{pl}L\sigma_{yz},\ \dot{\varepsilon}_{xz}=4\lambda^{pl}M\sigma_{xz}\end{aligned} \tag{24}$$

Using the analytical model detailed in the previous section, for the first position of the specimen (specimen S1) in the channel die compression device, the two equations (22) and (24) lead to:

$$\begin{aligned}&V/h=2\lambda^{pl}\left[-G\sigma^{(1)}_{ND//ND_0}-H\sigma^{(1)}_{TD//TD_0}\right]\\ &0=2\lambda^{pl}\left[F\left(\sigma^{(1)}_{TD//TD_0}-\sigma^{(1)}_{ND//ND_0}\right)+H\sigma^{(1)}_{TD//TD_0}\right]\text{i.e. }\sigma^{(1)}_{TD//TD_0}=\frac{F}{F+H}\sigma^{(1)}_{ND//ND_0}\\ &-V/h=2\lambda_{pl}\left[-F\left(\sigma^{(1)}_{TD//TD_0}-\sigma^{(1)}_{ND//ND_0}\right)+G\sigma^{(1)}_{ND//ND_0}\right]\end{aligned} \tag{25}$$

Then for all the three different positions, combining equations (12), (22), (24) and corresponding (25) ones, the following relationships can be easily obtained:

$$\sigma^{(1)^2}_{ND//ND_0}\left(\frac{FG+FH+GH}{F+H}\right)=1 \text{ for P1}$$

$$\sigma^{(2)^2}_{ND//ND_0}\left(\frac{FG+FH+GH}{G+H}\right)=1 \text{ for P2} \quad (26)$$

$$\sigma^{(3)^2}_{ND//TD_0}\left(\frac{FG+FH+GH}{F+G}\right)=1 \text{ for P3}$$

These three relationships lead to the following expressions of anisotropic criterion coefficients:

$$F=\frac{\alpha}{\alpha\beta+\beta\gamma+\gamma\alpha}\ ;\ G=\frac{\beta}{\alpha\beta+\beta\gamma+\gamma\alpha}\ ;\ H=\frac{\gamma}{\alpha\beta+\beta\gamma+\gamma\alpha} \quad (27)$$

where:

$$\alpha=\frac{1}{2}\left[\sigma^{(1)^2}_{ND//ND_0}+\sigma^{(3)^2}_{ND//TD_0}-\sigma^{(2)^2}_{ND//ND_0}\right],\ \beta=\frac{1}{2}\left[\sigma^{(2)^2}_{ND//ND_0}+\sigma^{(3)^2}_{ND//TD_0}-\sigma^{(1)^2}_{ND//ND_0}\right]$$

and

$$\gamma=\frac{1}{2}\left[\sigma^{(1)^2}_{ND//ND_0}+\sigma^{(2)^2}_{ND//ND_0}-\sigma^{(3)^2}_{ND//TD_0}\right] \quad (28)$$

The parameters *L*, *M*, *N* can be determined from simple shear tests (Liu *et al.,* 1997). Starting from the curves pictures in Fig. 9 and using the phenomenological law (1), the parameters defining the stress components in the ND_0 direction are identified using an inverse analysis technique based on a non-linear regression of a cost function describing in a least squares sense the difference between the experimental points and the predicted ones. The identification results are presented in the Table 3 (here W is chosen equal to 1).

Parameters	S1 (position 1)	S2 (position 2)	S3 (position 3)
σ_{00}	200.	254.	213.
σ_{pl}	538.519	714.260	459.817
n	3.607	1.239	7.563
n_a	0.5	0.5	0.5
Mean error (E_r)	2 %	1.60%	2.60%

Table 3. Identified parameters results obtained for the proposed phenomenological law corresponding to the chosen three positions of the samples (S1, S2 and S3 specimens).

Using the (16) and (17) expressions it is possible to obtain a variation of the Hill coefficients with the defined cumulated plastic strain i.e. $F(\bar{\varepsilon}), G(\bar{\varepsilon})$ and $H(\bar{\varepsilon})$. These evolutions of the Hill coefficients permit to make the classical anisotropic Hill criterion more consistent with the large plastic deformation phenomena which occur during the real forming process and to extend its availability for a large class of metallic materials.

In the particular case of a normal anisotropy, we must have $\frac{dr(\theta)}{d\theta} = 0$. Using formula (4), (16) and (17) it is necessary to have $N=F+2H$ and $F = G$ i.e. $\sigma^{(1)}_{ND//ND_0} = \sigma^{(2)}_{ND//ND_0}$. Or the variation of the stress plotted in Fig. 9 shows that between 10% and 30% of the cumulated plastic strain, this condition is rigorously reached. Then, the corresponding Hill coefficients have the following analytical expressions:

$$F = G = \frac{2}{4\sigma^{(1)2}_{ND//ND_0} - \sigma^{(3)2}_{ND//TD_0}},\ H = \frac{2\left[2\sigma^{(1)2}_{ND//ND_0} - \sigma^{(3)2}_{TD//ND_0}\right]}{\sigma^{(3)2}_{ND//TD_0}\left[4\sigma^{(1)2}_{ND//ND_0} - \sigma^{(3)2}_{ND//TD_0}\right]} \quad (29)$$

According to the proved normal anisotropy assumption, for a plan stress hypothesis, the anisotropic criterion in the local (x, y) axes of the plate can be written in the following form:

$$\sigma^2_{xx} + \sigma^2_{yy} - \frac{2r}{r+1}\sigma_{xx}\sigma_{yy} + \frac{2(2r+1)}{r+1}\sigma^2_{xy} = \frac{2r+1}{2(r+1)}\sigma^{(3)2}_{ND//TD_0} = \sigma^2_0 \quad (30)$$

where *r* is named here the Lankford coefficient and can be expressed by:

$$r = r(0) = R = \frac{H}{G} = 2\frac{\sigma^{(1)2}_{ND//ND_0}}{\sigma^{(3)2}_{ND//TD_0}} - 1 \quad (31)$$

With these expressions the dependence of the Lankford coefficient with the cumulated plastic deformation (defined by (20)) can be predicted from the stress-strain curves determined in the previous section. The dependence of the stress components with plastic deformation is given by (17) (see also Table 3). The values predicted by the model are expected to be more realistic when the plastic deformation is relatively low (such as in the case of the tensile test). The result is presented in Fig. 10. For a low plastic deformation (< 5%), it can be seen that the values of *r* are close to 0.57. This value is consistent with the experimental value of *r(0)* =0.54 near determined for θ = 0° (see Fig. 8). The values increase with the plastic deformation: for 25% of deformation, *r* is near 0.9 and the variation is asymptotic to 1 for more large plastic strains. The range of these values is consistent with those mentioned for aluminium alloys [9, 15] and it can be concluded that the proposed model predicts the Lankford coefficient values in accordance with the known anisotropic material properties of AA 2024 alloy. Moreover, the evolution of σ_0 with plastic deformation presented in Fig. 10 shows that the obtained increasing variation is coherent for this material and realistic with other experimental previsions.

8. Conclusions

Channel die compression tests have been carried out for the characterization of the anisotropy of an aluminium alloy undergoing large plastic deformations. Crystallographic evolutions and stress-strain curves show that the material has a specific response according to the normal plane of compression of the specimen. Significant differences are measured

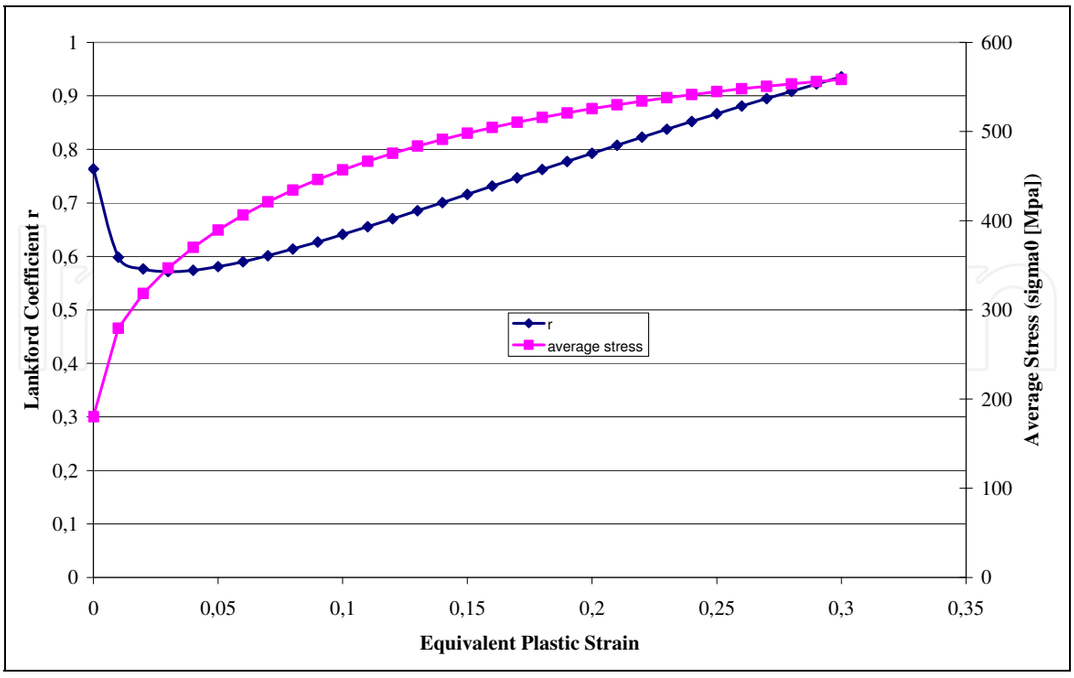

Fig. 10. Prediction of the variation of the Lankford coefficient and of the σ_0 with the equivalent plastic deformation.

when the normal plane is along TD_0 and the longitudinal direction along LD_0. An analytical model, adapted for the channel die compression test, has been proposed in order to describe a Hill criterion. This proposed analysis permits to have an analytical expression of the Hill coefficients and the new idea is here the introduction of its variations with the plastic strain values. The realistic prediction of the Lankford coefficient evolution shows that the obtained values are consistent with values measured for general aluminium alloys. In a future work new 3D anisotropic criteria will be analyzed for plastic solid materials starting from this study and using all the six possible positions of the plate specimen in the channel die compression device.

9. References

Banabic, D.; Bunge, H. –J.; Pöhlandt, K. & Tekkaya, A. E. (2000). *Formability of Metallic Materials: Plastic Anisotropy, Formability Testing, Forming Limits,* Springer-Verlag Berlin and Heidelberg GmbH & Co. K.

Banabic D.; Cazacu, O.; Barlat, F.; Comsa, D. S.; Wagner, S. & Siegert, T. (2002). Description of anisotropic behaviour of AA3103-0 aliminium alloy using two recent yeld criteria, *6th EUROMECH-MECAMAT*, pp. 297-304, Liège, Belgium, 9-12 September 2002, edited by S. Cescotto, C. Teodosiu, A.-M. Habraken, R. Billardon and I. Doghri.

Bacroix, B. & Jonas, J. J. (1998). Proc. ICOTOM 8, pp. 403-421, J.S. Kallend, G. Gottstein (Eds.), Warrendale, The Metallurgical Society.

Barralis J. & Maeder, G. (2005). *Précis de Métallurgie,* Nathan Eds.

Baudelet, B.; Deguen, M.; Felgères, L.; Parnière, P.; Roné-Oustau, F. & Sanz, G. (1978). *Mém. Scient. Revue Métall.,* 75, 409-422.
Bishop, J. F. W. & Hill, R. (1951). *Phil. Mag.,* 42, 414, 1298.
Bishop, J. F. W. (1953). *Phil. Mag.,* 44, 51.
Browen, A. W. (1990). *Mater. Sci. Technol.,* 11, 1058-1071.
Bunge, H. J. (1996). Texture Analysis in materials science, London, Butterworth.
Bunge, H. J. & Schwarzer, R. (1998). Orientation stereology – a new branch of texture studies, *TU Contact* (Clausthal), 2, 67-73.
Cazacu, O. & Barlat, F. (2001). *Mathematics and Mechanics of Solids*, 6, 613-630.
Chin, G. Y. & Mammel, W. L. (1969). *Trans. Metall. Soc. AIME.,* 245, 1211.
Choi, S.-H. & Barlat, F. (1999). Prediction of macroscopic anisotropy in rolled aluminium-lithium sheet, *Scripta Mater.,* 41, 981-987.
Choi, S. H.; Brem, J. C.; Barlat, F. & Oh, K. H.(2000). *Acta mater,* 48, 1853-1863.
Choi, S. H.; Barlat, F. & Liu, J.(2001). *Metallurgical and Materials Transactions A,* 32A, 2239-2247.
Engler, O.; Hecklmann, I.; Rickert, T.; Hirsch, J. & Lücke, K. (1994). *Mater. Sci. Technol.,* 10, 10, 771-781.
Engler, O.; Hirsch, J. & Lücke, K. (1995). *Acta Metall.,* 43, 1, 121-138.
Engler, O.; Crumbach, M. & Li, S. (2005). *Acta Mater.,* 53, 2241-2257.
Fjeldl, A. & Roven,A. (1996). Observations and calculations on mechanical anisotropy and plastic flow of an AlZnMg extrusion, *Acta Mater.*, 44, 9, 3497-3504.
Francillette, H.; Castelnau, O.; Bacroix, B.;J Béchade, J. L.(1998). Experimental and predicted texture evolutions in zirconium alloys deformed in channel die compression, *Mat. Science Forum*, 273-275, 523-528.
Francillette, H.; Gavrus, A. & Lebensohn, R. A.(2003). A constitutive law for the mechanical behaviour of Zr702□, *Journal of Materials Processing Technology,* 142, 43-51.
Gavrus, A.(1996). *Identification automatique des parameters rheologiques par analyse inverse,* PhD Thesis, Ecole des Mines de Paris Eds, France.
Hansen, J.; Pospiech, J. & Lücke, K. (1978), *Tables for textures. Analysis of cubic crystals,* Berlin, Springer.
Hansen, N. (1991). Distributions of glide systems in cell formation metals. In : T. C. Lowe, A. D. Rollett, P. S. Follansbee & G. S. Daehn (Eds), Modelling the Deformation of Crystalline Solids, pp. 37-49, TMS, Warrendale,.
Hansen, N. (1992). *Scr. Metall. Mater.,* 27, 947-950.
Hill, R.(1948). A theory of the yielding and plastic flow of anisotropic metals. *Proc. Roy. Soc. London A,* 193, 281.
Hill, R. (1979). *Math. Proc. Camb. Phil Soc.,* 85.
Hirsch, J. & Lücke, K. (1988). *Acta Metall.,* 36, 2883-2904.
Hu, H. & Cline, R. S. (1961). *J. Appl. Phys.,* 32, 760.
Hu, H. & Goodman, S. R. (1963). *Trans. Metall. Soc. AIME,* 227, 627.
Hu, J.; Ikeda, T. & Murakami, T. (1998). *Journal of Materials Processing Technology,* 73, 49-56.
Hughes, D. A. (1992). *Scr. Metall. Mater.,* 27, 969-974.
Hughes, D. A. (1993). *Scr. Metall. Mater.,* 41, 1421-1430.
Huh, M. Y.; Cho, S. Y. & Engler, O.(2001). Randomization of the annealing texture in aluminium 5182 sheet by cross-rolling, *Materials Sciences and Engineering A,* 315, 35-46.

Jin, H. & Lloyd, D. J.(2005). *Materials Sciences and Engineering A*, 399, 358-367.

Khalffalah, A. (2004). *Identification des lois de comportement élastoplastiques par essais inhomogènes et simulations numériques,* PhD Thesis, Université Tunis El Manar, Tunis.

Kuwabara, T.; Van Bael, A. & Iizuka, E. (2002). *Acta Mater.,* 50, 3717-3729.

Lademo, O.-G.; Hopperstad, O.S. & Langseth, M. (1999). *International Journal of Plasticity*, 15, 191-208.

Leacock, A. G. (2006). *Journal of the Mechanics and Physics of Solids,* 54, 425 –444.

Lebensohn, R. A. & Tomé, C. (1993). *Acta Metall.,* 41, 2611-2624.

Lequeu, Ph.; Gilormini, P.; Montheillet, F.; Bacroix, B. & Jonas, J. J. (1987). *Acta Metall.,* 35, 5, 1159-1174.

Li, Z. J.; Winter, G. & Hansen, N. (2004). Anisotropy of plastic deformation in rolled aluminium, *Mat. Sci. Eng. A*, 387- 389, 199-202.

Liu, C.; Huang Y. & Stout, M. G. (1997). On the asymmetric yield surface of plastically orthotropic materials: a phenomenological study, *Acta Mater,* 45, 6, 2397-2406.

Lopes, A. B.; Barlat, F.; Gracio, J. J.; Ferreira Duarte, J. F. & Rauch, E. F. (2003). *Int. J. Plast. ,* 19,1-22.

Lücke, K. & Engler, O. (1990). *Mater. Sci. Technol.,* 6, 11, 1113-1130.

Lloyd, D. J. & Kenny, D. (1980). The structure and properties of some heavily cold worked aluminium alloys, *Acta Metallurgica*, 28, 639-649.

Malo, K.A.; Hopperstad, O.S. & Lademo, O.G. (1998). J. *of Mat. Processing Technology*, 80-81, 538-544.

Molinari, A.; Canova, G. R. & Ahzi, S. (1994). *Acta Metall. Mater.,* 42, 2453.

Park., J.-J. (1999). Predictions of texture and plastic anisotropy developed by mechanical deformation in aluminium sheet, *Journal of Materials Processing Technology*, 87,146-153.

Sachs, E. (1928). *Z. Ver. Dt. Ing.,* 72, 734.

Taylor, G. I. (1938). *J. Inst. Met.,* 62, 307.

Tong, W. (2006). A plane stress anisotropic plastic flow theory for orthotropic sheet metals, *Int. J. of Plast.,* 22, 497-535.

Yoon, J. W.; Barlat, F.; Gracio, J. J. & Rauch, E. (2005). Anisotropic strain hardening behaviour in simple shear for cube textured aluminium alloy sheets, *International Journal of Plasticity,* 21, 2426-2447.

Zeng, X. H.; Ahmad, M. & Engler, O. (1994). *Mater. Sci. Technol.*, 10, 7, 581-591.

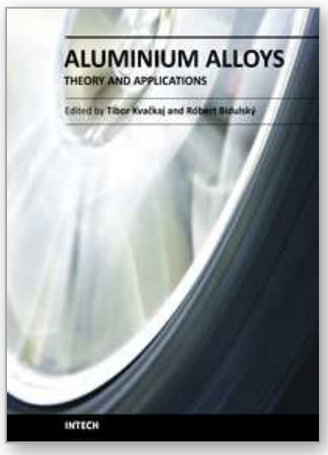

Aluminium Alloys, Theory and Applications

Edited by Prof. Tibor Kvackaj

ISBN 978-953-307-244-9
Hard cover, 400 pages
Publisher InTech
Published online 04, February, 2011
Published in print edition February, 2011

The present book enhances in detail the scope and objective of various developmental activities of the aluminium alloys. A lot of research on aluminium alloys has been performed. Currently, the research efforts are connected to the relatively new methods and processes. We hope that people new to the aluminium alloys investigation will find this book to be of assistance for the industry and university fields enabling them to keep up-to-date with the latest developments in aluminium alloys research.

InTech Europe
University Campus STeP Ri
Slavka Krautzeka 83/A
51000 Rijeka, Croatia
Phone: +385 (51) 770 447
Fax: +385 (51) 686 166
www.intechopen.com

InTech China
Unit 405, Office Block, Hotel Equatorial Shanghai
No.65, Yan An Road (West), Shanghai, 200040, China
中国上海市延安西路65号上海国际贵都大饭店办公楼405单元
Phone: +86-21-62489820
Fax: +86-21-62489821

IntechOpen